Human Rad52 binding renders ssDNA unfolded: image and contour length analyses by atomic force microscopy

Jacinta S. D'Souza, Jayashree A. Dharmadhikari, Aditya K. Dharmadhikari, Vasundhara Navadgi, Deepak Mathur and Basuthkar J. Rao*

Tata Institute of Fundamental Research, 1 Homi Bhabha Road, Mumbai 400 005, India

Atomic force microscopy imaging has been used to study the changes associated with human Rad52 (HsRad52) protein in solution, in dried state as well as following ssDNA (linear and circular) binding. In the dried state, the free protein exists predominantly as a characteristic panoply of novel trifoliate forms. However, in solution, the level of trifoliates diminishes significantly. Height analyses of either form reveal two categories: smaller (~ 3–5 nm) and larger (~ 10–12 nm) particles, perhaps related to sub-heptameric and heptameric forms respectively. Interestingly, binding of the protein to linear ssDNA smoothly extends and unfolds the naked DNA. Contour length measurements performed on several individual circular ssDNA/nucleoprotein complexes reveal marked (about threefold) extension of naked ssDNA, following HsRad52 binding. We speculate that the alignment of HsRad52 on ssDNA into a smoothly extended and unfolded strand from that of highly compact morphology of naked ssDNA, may have bearing on the recombination function of HsRad52 protein.

Keywords: Atomic force microscopy, DNA contour length, protein–DNA interaction, Rad52 protein, recombination.

GENOMIC integrity maintenance and the stable transmission of genetic sequences depend on a number of DNA repair processes. Failure to staunchly perform these processes can result in genetic mutations and consequent occurrence of genetic diseases or lethality. Also, genetic instability is characteristic of cancer cells, both at the chromosomal level (e.g. aneuploidy, aneusomy, translocations), and at the sequence level (e.g. microsatellite instability). Agents that cause damage to DNA are varied, such as ionizing irradiation, ultraviolet rays, oxygen radicals, etc. In turn, the types of lesions that happen to DNA are also diverse; deamination, mismatches of the normal bases because of a failure of proofreading during DNA replication, breaks in the backbone (a single-stranded break (SSB) or a double-stranded break (DSB), and crosslinks (covalent linkages can be formed between bases)). Mutations in DSB repair genes are often lethal. Remarkably, many of the viable mutations in DSB repair factors lead to accelerated aging and premature senescence in culture, which further supports the role of DSB repair in aging[1]. Data from a large number of mice harbouring mutations in DNA damage response genes are available and have been important for valuable insights into DNA repair and human disease[2,3].

One of the biological processes important to life is homologous recombination[4]. It involves an efficient and error-free pathway of repairing DNA DSBs, presumed to be the most deleterious of DNA lesions. The important molecules central to the process of homologous recombination are the RAD52 epistasis group of genes (*RAD50*, *RAD51*, *RAD52*, *RAD54*, *RDH54/TID1*, *RAD55*, *RAD57*, *RAD59*, *MRE11* and *XRS2*), most of which were identified by their requirement for the repair of ionizing radiation-induced DNA damage in *Saccharomyces cerevisiae*[5]. Recent studies showing defects in homologous recombination and double-strand break repair in several human cancer-prone syndromes have highlighted the importance of this repair pathway in maintaining genome integrity[6].

The Rad52 group of proteins is highly conserved among eukaryotes, and Rad51, Mre11, and Rad50 are also conserved in prokaryotes and archaea[7]. Many of the enzymes that are involved in recombination have been isolated, the crystal structures for some have been obtained, and details are in the process of being unravelled. The open reading frame of the human *RAD52* gene encodes a protein of 418 amino acids. In humans, the *RAD52* gene seems to be indispensable for homologous recombination and DNA repair. Human Rad52 protein (HsRad52) binds DNA, promotes single strand DNA annealing[8,9] and three-stranded pairing[10] that may, in some conditions, lead to strand exchange[11]. The primary function of Rad52 is to stimulate Rad51-mediated homologous pairing by facilitating its recruitment to ssDNA[12,13]. While HsRad52 physically interacts with other proteins involved in recombination, such as HsRad51, RPA, etc.[12–16], it also contains domains of self-association and those that lead to the formation of higher order structures[17]. The protein

*For correspondence. (e-mail: bjrao@tifr.res.in)

exhibits the ability to assemble into ring-like structures, as visualized by electron microscopy[8,17–21]. Using both conventional and scanning transmission electron microscopy, the HsRad52 protein has been observed to form heptameric rings. Elegant studies related to three-dimensional reconstruction have revealed that the heptamer has a large central channel[20]. Recent high-resolution crystal structures reveal that C-terminally deleted form of HsRad52 also forms a ring-shaped undecameric oligomer of ~ 12 and ~ 6 nm diameter and height respectively, where the top-rim of the 'mushroom-like ring' is expected to lodge a composite binding site for both ss and dsDNA[9,22]. It is believed that the undecameric ring-shaped oligomer is structurally as well as functionally equivalent to heptameric rings formed by full-length protein subunits.

Atomic force microscopy (AFM) has, in recent years, been of much utility in studies of processes as diverse as local nano-mechanical motions in yeast[23] to the architecture of proteins involved in DNA repair[24–26], recombination[27–29] and regulation of nucleosomal remodelling events[30]. It has also been used to determine the binding affinity, specificity and stoichiometry, as well as the conformational properties of the protein–DNA complexes[31]. Protein–protein[32] and protein–DNA interactions have been studied using the AFM. Most AFM studies related to protein–DNA complexes reported so far were done on dsDNA rather than ssDNA, where the former, even as naked strands, yields a much clearer image than the latter[33–35]. In this article, we have used AFM to probe the HsRad52 protein system for studying the changes associated with various aggregated states of protein, free as well as ssDNA bound, and its effect upon DNA binding. In liquid conditions, a state that is closer to the physiological conditions and where the protein was found to be biochemically active, HsRad52 exists either as sub-heptameric (~ 3–6 nm height) or heptameric (~ 10 nm height) particles, which in air-dried state reveal as uniquely characteristic particles of similar heights, but as trifoliate-shaped structures, not seen earlier by other methods. Image analyses of nucleoprotein complexes formed with linear ssDNA fragments reveal unfolded DNA that is extensively coated with protein particles. Interestingly, contour length measurements performed on several individual circular ssDNA/nucleoprotein complexes revealed about three- to four-fold extension of naked ssDNA, following HsRad52 binding. Based on this data, we speculate that the alignment of HsRad52 on ssDNA into a smoothly extended and unfolded strand may have a bearing on the recombination function of HsRad52 protein.

Methods and materials

Materials

The HsRad52 protein was overexpressed as a His-tagged full-length protein and purified using Ni-NTA affinity chromatography, as has been described in detail recently[10].

Sample preparation for AFM imaging

Free (DNA-unbound) protein: A 30 μM stock of purified HsRad52 protein was diluted to 0.8 μM in the deposition buffer containing 10 mM HEPES-KOH (pH 7.6) and 2.5 mM $MgCl_2$. A 200 μl aliquot was spotted onto freshly cleaved mica (SPI), left for 5 min and then imaged using atomic force microscope (PicoScan, Molecular Imaging USA) in non-contact AC mode with a liquid cell. The same sample was left overnight to dry slowly and then imaged in the non-contact AC mode. A silicon cantilever tip with a resonance frequency of 80 kHz and spring constant 5 N/m was used for imaging the sample.

Free ssDNA: M13 ssDNA fragments were prepared by several cycles of freeze–thawing of circular M13 ssDNA. The fragments showed a large size distribution on the gel assay (data not shown). Intact M13 DNA, containing > 95% molecules as circular form (by gel assay), was also used. The DNA sample was diluted in the deposition buffer to a final concentration of 0.5 μg/ml and imaged in the same manner as described above for both dry and liquid conditions. For circular free ssDNA, see sample spotting and imaging conditions below.

ssDNA–protein complexes: Linear ssDNA fragments and protein samples were mixed at a ratio of 1 : 1 (1 μM each of protein and DNA nucleotide), incubated in the incubation buffer (30 mM Tris-acetate, pH 7.5, 1 mM $MgCl_2$, 1 mM DTT) at 37°C for 30 min, diluted 200-fold in the deposition buffer and then imaged in the tapping mode under liquid conditions. Circular M13 ssDNA and protein were incubated (37°C for 10 min) at a ratio of DNA : Protein 1 : 1 (1 μM each of protein and DNA nucleotide) in the incubation buffer. After incubation, glutaraldehyde was added to a final concentration of 0.2% and the mixture further incubated at 37°C for 20 min. An aliquot of 12 μl of the 1 : 200 diluted (in deposition buffer) incubation mixture was then deposited on freshly cleaved mica. The nucleoprotein complexes were allowed to dry overnight at RT, washed with deposition buffer and then purged with argon gas. For comparison, circular M13 DNA was also incubated in a similar manner, except that it was incubated without HsRad52 protein, diluted in the deposition buffer to a final concentration of 0.5 μg/ml, and then imaged in air at room temperature and humidity in the contact mode.

Image analyses: All the images were analysed using standard image analysis software (SPIP, from Image Metrology, Denmark) that corrected for plane distortions and provided histograms for height distributions. The particle heights were measured at random intervals from several

image scans of the DNA strands or free proteins. ImageJ program was used for contour length measurements of circular ssDNA as well as circular nucleoprotein complexes. Tracings drawn along the midline of a circular contour image of ssDNA/nucleoprotein complex yielded the number of pixels for the contour, which was then converted into nanometres by normalizing against the image scan size. Repeated contour length measurements thus obtained for the same circular image did not vary by more than 5%. In all, 70–100 random images were measured for heights and contour lengths.

Dynamic light scattering measurement of hydrodynamic radius: Dynamic light scattering (DLS) experiments were performed at 22°C on a DynaPro-MS800 dynamic light scattering instrument (Protein Solutions Inc., VA, USA) having an in-built laser at 820 nm, by monitoring the scattered light at 90° with respect to irradiation direction. Buffer solutions were filtered carefully through 20 nm filters (Whatman Anodisc 13) to remove dust particles. The observed autocorrelation curves (at least ten collections each collected for 10 s) were analysed either by Regularization software or DynaLS software provided by the manufacturer of the instrument to generate a distribution of R_h. Synthetic beads of 6 nm diameter (provided by Protein Solutions Inc.) and bovine serum albumin (3 nm) were used as standards. A typical DLS experiment involved the addition of reaction buffer (50 µl) (10 mM HEPES-KOH (pH 7.6) and 2.5 mM $MgCl_2$) to the quartz cuvette, followed by ascertaining that the buffer system is free of particles as reflected by very low R_h (0.1–0.2 nm) values associated with it. A small aliquot (1–2 µl) of stock protein sample that is cleared of particles by prior quick centrifugation, is added to the buffer (the final concentration of protein was ~ 1.0 µM), followed by collection of light scattering autocorrelation curves to obtain distribution of R_h.

Results and discussion

Elegant studies involving electron microscopy combined with image reconstructions as well as high-resolution crystallography of HsRad52 protein have delineated rich structural information about the protein system[17–19]. Three-dimensional reconstruction of several electron micrographs revealed that the full-length protein exists as a heptameric ring (diameter of ~ 10 nm and height of ~ 11 nm) possessing a central hole[20]. The crystal structure of the N-terminal domain (residues 1 to 212) of the HsRad52 protein has shown an 11-member ring of about 10 nm diameter and 6.5 nm height[9,22]. In light of the existing structural information of free protein (unbound to DNA), what remains unclear is the nature of its organization in the ssDNA–protein complex and importantly, how protein binding affects the configuration of ssDNA to enable the recombination function. Therefore, the current AFM study complements the already existing high-resolution structural information and aims to provide overall organizational understanding of the system that relates to function.

AFM imaging of free (unbound to DNA) HsRad52 protein

The protein solution conditions chosen were such that HsRad52 efficiently binds ssDNA and forms pairing competent complexes[10,36,37]. Imaging was carried out in solution as well as dried liquid samples spotted on the mica surface (see Methods). Purified HsRad52 protein, under liquid conditions exhibited images of randomly distributed protein 'particles' in a 5×5 µm scan. Several such images were scanned at various positions on the mica surface. A typical 2D image reveals distribution of particles with varying sizes (Figure 1 *a*). Height measurements revealed particles of ~3 to 6 nm and a few of ~ 10 nm height (Figure 1 *b–d*). Interestingly, when the same sample preparation was analysed for hydrodynamic radii (R_h) in solution using the DLS method, a much wider distribution of R_h (~ 10–100 nm) was evident, suggesting that in solution the protein particles (of the type imaged in AFM) perhaps further aggregate loosely into much bigger light scattering centres (Figure 1 *e*). We therefore tend to believe that AFM sample preparation involving adhesion onto mica surface might dissociate such loosely held protein aggregates.

Similar distribution of sizes was observed when the sample was air-dried prior to AFM imaging (Figure 2). However, the air-dried samples exhibited significant difference by revealing a unique morphology of 'trifoliate' forms (Figure 2 *a, d*), where quantitation revealed that characteristic panoply of trifoliate-like forms was abundant (~ 90–95%) and only a few non-trifoliate forms were found in a large collection of images. In contrast, the trifoliates were observed in only 5% of the scans that were conducted under liquid conditions described in Figure 1. A typical trifoliate particle revealed three 'lobes', which appeared in the shape of a cloverleaf, placed side by side, seeming to meet at the centre (Figure 2 *d*). The height distribution of particles revealed a wide range: smaller to medium trifoliates of ~ 2–6 nm height and large ones of ~ 10–12 nm height (Figure 2 *b, c*). Irrespective of varying heights, the distinct trifoliate form was inescapably evident.

All the data on particle heights suggest that HsRad52 protein seems to exist in multiple oligomeric states, which is consistent with the existing data in the literature. A comprehensive analysis of EM-images revealed that the HsRad52 protein, in addition to ring-shaped oligomers (9–13 nm diameter), has forms that are consistent with broken C-shaped half rings or compressed forms of rings leading up to the occurrence of higher order aggregates (30–100 nm)[8,17–22]. In the current AFM images, the distri-

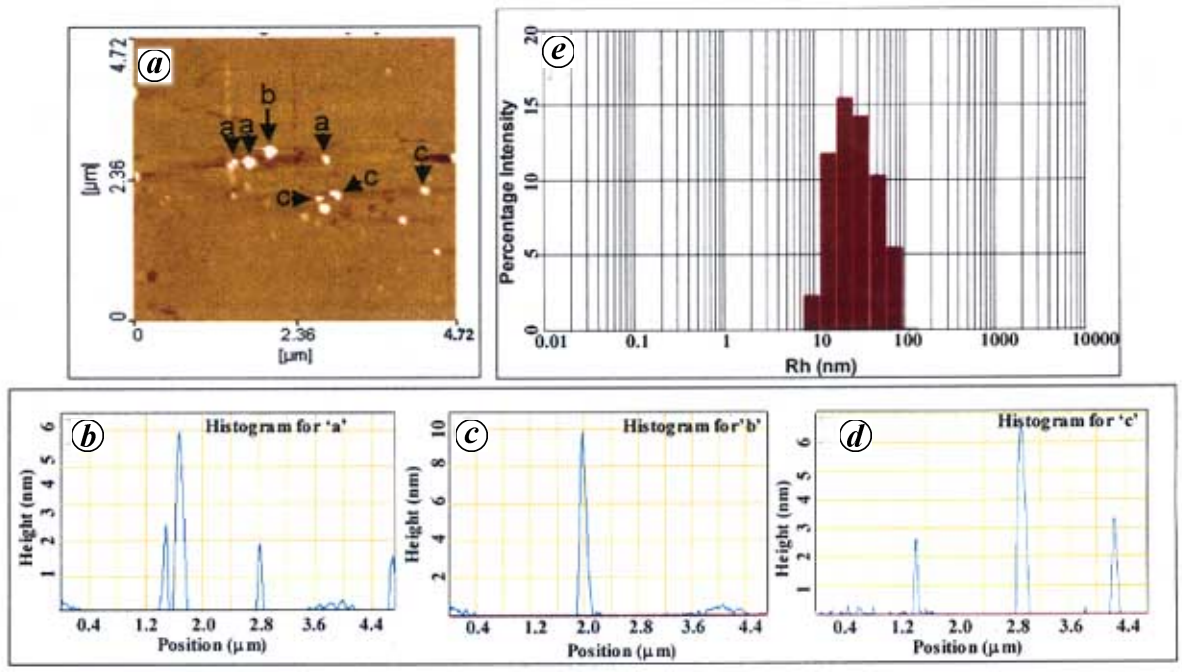

Figure 1. Atomic force microscopy imaging of 0.8 µM HsRad52 under liquid conditions. ***a***, is a 2D scan (5 × 5 µm) in which representative particles are indicated by a, b and c. ***b–d***, Graphical representation of distribution of heights (in nm) along various lines encompassing the protein particles indicated by a, b and c respectively, in (***a***). The distribution of heights is plotted as a function of its position in the image scan. All the heights of protein particles here as well as in other figures are expressed after plane correction. ***e***, Analyses of hydrodynamic radii of HsRad52 by dynamic light scattering method. Distribution of particle hydrodynamic radii (R_h) versus their frequencies, generated by a set of autocorrelation curves obtained for HsRad52 (~ 1.0 µM) protein solution (see Methods).

bution of protein particles revealed a significant fraction of forms that appear much smaller than what one expects of full-length heptameric rings. However, lack of sufficient resolution does not allow us to decipher the intact or broken rings, but the accuracy of the height analyses enabled us to relate the particles to the known forms described in the literature, with one strong exception. Our data on dried samples show an abundance of trifoliate forms, which were not evident in earlier studies. Since the AFM has the ability to non-destructively image soft biological matter under liquid and dry states, close to physiological conditions without sample fixation, we see trifoliate-like structures as well as preponderance of several structures of differing heights, where the particles of maximum heights (~ 10–12 nm) might relate to the known heptameric/undecameric ring-shaped structures.

AFM imaging of DNA-bound HsRad52 protein

Nucleoprotein complexes on linear ssDNA: We then studied protein oligomeric states on ssDNA–protein complexes. A mixture of DNA fragments obtained from M13-ssDNA was used for protein binding. We ascertained protein binding to ssDNA by classical gel-shift analysis of ssDNA as a function of protein concentration (Figure 3 *a*). The experiment revealed that by about ~ 0.5 µM protein concentration, essentially all ssDNA molecules were bound by protein, as no free DNA was visible. At this condition, protein monomer to ssDNA nucleotides molar ratio being about 1 : 1, a condition of excess protein compared to that required according to binding stoichiometry, implied full coating of ssDNA by protein[10,17,20]. We imaged these ssDNA–protein complexes in liquid by AFM, which revealed that following the saturated binding of protein, the mixture of ssDNA strands appeared highly unfolded and stretched out (Figure 3 *b*). Under these conditions of imaging, naked linear DNA revealed as highly condensed aggregates (data not shown), where individual ssDNA fragments were hardly visible, as opposed to circular ssDNA which revealed individual circular forms that were amenable for contour length measurements (see Figure 4). Interestingly, aggregates of naked ssDNA fragments were largely eliminated following protein addition and further led to the formation of highly unfolded nucleoprotein complexes (Figure 3 *b*). The morphology of such protein coated ssDNA showed distinct beaded appearance essentially all along the strand where the available resolution would not allow a clear demarcation of naked ssDNA stretches, if any, from those of protein-bound DNA regions. However, distinctly particulate protein regions associated with ssDNA (marked with arrowheads in Figure 3 *b*) were analysed for heights. The analyses revealed 5–6 nm heights, with a conspicuous absence of ~ 10 nm high particles found in free protein images (Figures 1 *b* and 2 *b*, *c*). In addition, ssDNA–protein sample images revealed a

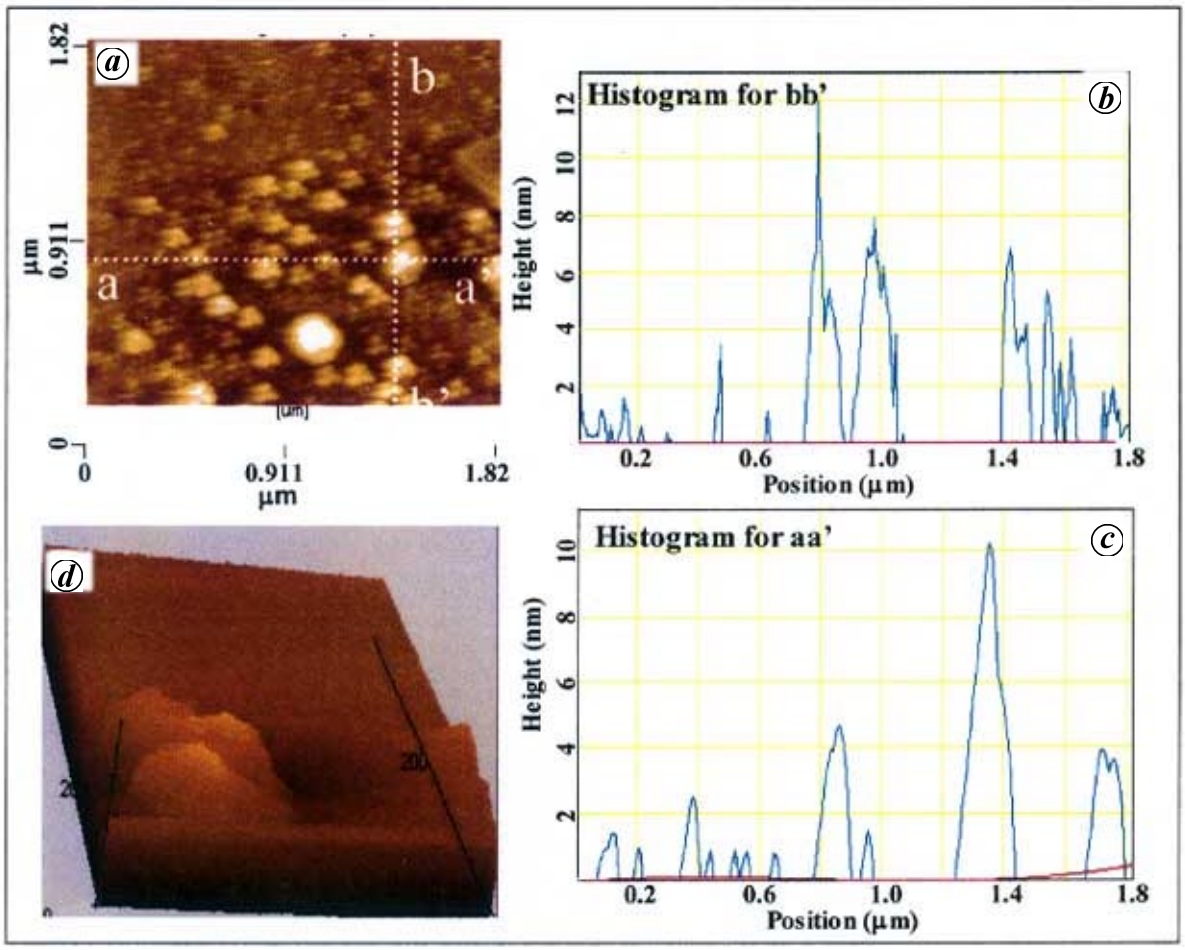

Figure 2. Atomic force microscopy imaging of 0.8 µM HsRad52 in air. ***a***, Representative 2D image (2 × 2 µm) with the trifoliate-like structures. Dotted lines (aa′ and bb′) represent chosen lines along which height distribution in analysed. ***b***, ***c***, Graphical representation of the trifoliate heights recovered along bb′ and aa′ axes respectively, of image shown in (***a***). ***d***, Representative 3D image (300 × 300 nm) of a single trifoliate.

higher background of much smaller protein particles compared to that of free protein sample images (compare scans *c–e* of Figure 3 with *b–d* of Figure 1). Moreover, the observed smaller protein particles in the scans appeared largely to belong to those that are not associated with ssDNA strands. These changes reflecting 'disaggregation' of HsRad52 protein particles following the addition of ssDNA are entirely consistent with biochemical data, where we have earlier shown large-scale 'solublization' of protein aggregates by ssDNA leading even to HsRad52 protein monomerization[37].

It is known that purified Rad52 protein binds preferentially to ssDNA and promotes annealing of complementary ssDNA[8–10]. Also, studies have shown preferential binding to the ends of ssDNA of tailed duplex molecules[38]. The terminal nucleotide is protected, and the region of ssDNA bound shows highly regular sensitivity to hydroxyl radicals. The periodicity of the hydroxyl radical sensitivity of DNA within the Rad52–DNA complexes is thought to be due to wrapping of ssDNA on the outside of the Rad52 ring[39].

Nucleoprotein complexes on circular ssDNA: Contour length analyses

As stated above, high aggregation propensity of naked ssDNA fragments disallowed contour length measurement, which was circumvented by studying the same using intact circular ssDNA molecules, where images revealed distinct circular contours (Figure 4 *a*). The basis of contrasting behaviour between ssDNA fragments and intact circular ssDNA is not clear and is a subject of separate ongoing study. The contour lengths measured on several individual circular molecules showed a distribution that ranged to about 400 ± 50 nm of circumference (see Methods and Figure 4 *d*, legend). This value was considerably less than that expected of the ~ 6400 nt long DNA strand, which assuming B-form helical parameters, when fully unfolded should yield about 2100 nm circumference. The 4–5-fold deficit recovered (400 ± 50 nm as opposed to ~ 2100 nm) is ascribable to high secondary as well as the tertiary folding associated with ssDNA. We next studied changes in the contour lengths, if any, brought about by

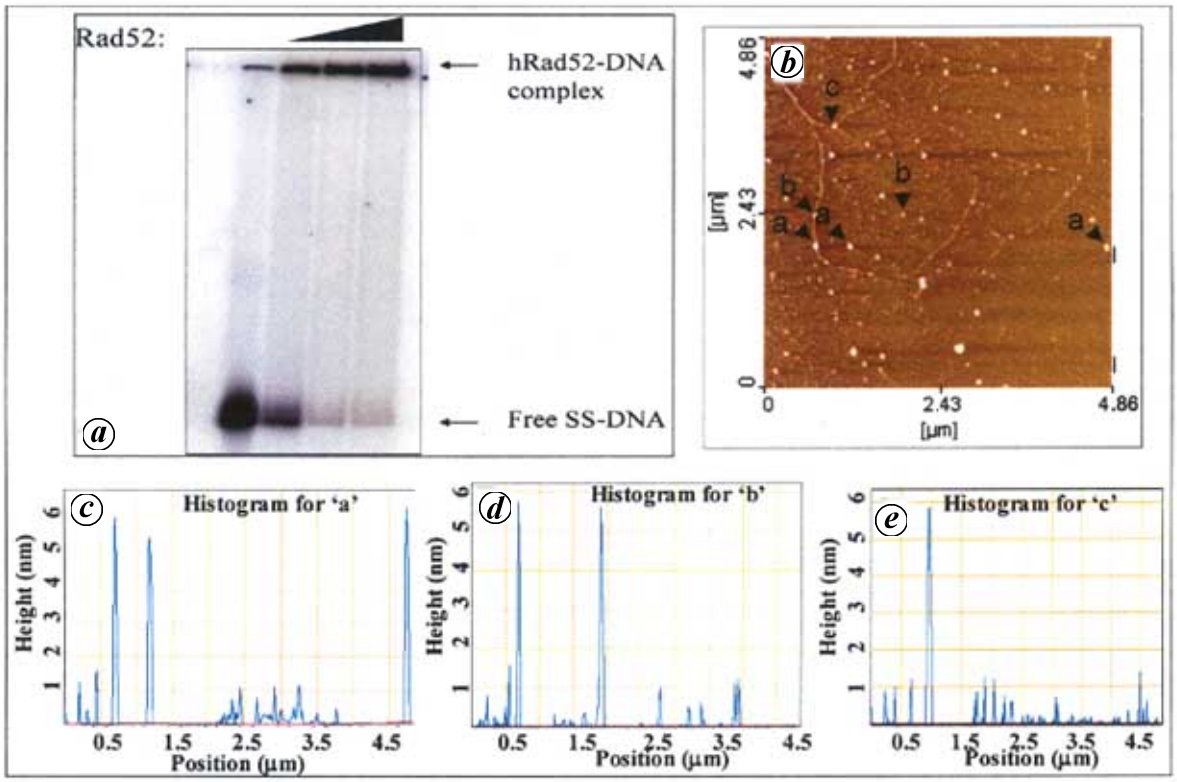

Figure 3. Unfolding of linear M13 ssDNA in the presence of HsRad52. ***a***, ssDNA binding analyses of HsRad52 by agarose gel assay. M13-ssDNA fragments (~2 μM nucleotides) were titrated with increasing levels of HsRad52 protein (0, 0.5, 1.0, and 2.0 μM), followed by analyses of the complexes by an agarose gel assay. ***b***, Atomic force microscopy imaging of HsRad52 in the presence of ssDNA fragments performed under liquid conditions. A representative 2D image (5 × 5 μm) of the 'unfolded' ssDNA fragments in the presence of hRad52, where arrowheads a, b and c indicate representative particles. ***c–e***, Graphical representation of distribution of heights (in nanometres) along various lines encompassing the protein particles indicated by a, b and c respectively in 2D image (***b***). Distribution of heights is plotted as a function of its position in the image scan.

HsRad52 protein binding to circular ssDNA. In order to study this, nucleoprotein complexes were stabilized further by fixation, prior to AFM imaging. Fixation step on naked circular ssDNA led to no substantial change in the overall size of DNA molecules, but gave rise to changes in the ultrastucture such that DNA images lost the central holes (Figure 4 *b*). Interestingly, when fixed nucleoprotein complexes were imaged, the circularity in the contours was fully regained (Figure 4 *c*). Moreover, comparison of scanned images, performed under identical scan conditions, revealed that nucleoprotein complexes are significantly larger in their circular contours compared to both fixed as well as unfixed ssDNA. Contour length measurements on several individual nucleoprotein complexes revealed circumference values in the range ~ 1200 ± 200 nm, which was about three fold higher than that of naked ssDNA (Figure 4 *d*). We assumed that height parameter would be particularly sensitive to the fixation related effects and hence height measurements were not carried out on these complexes. These analyses suggest that HsRad52 binding to ssDNA gives rise to substantial changes in DNA chain leading to unfolded state of DNA (Figures 3 *b*, and 4 *c*, *d*), a change perhaps important for its recombination function.

Conclusion

The sizes of HsRad52 protein oligomers uncovered in the present study suggest interesting organizational possibilities: Free protein exhibits forms with different particle heights, some of which (of height ~ 10 nm) might relate to classical heptameric, while the smaller ones (height 3–6 nm) to sub-heptameric forms of protein (Figure 1 *b–d*). The same units seem to coalesce into trifoliate (in dry samples) or non-trifoliate forms (in liquid samples). If one extends the analogy of heptamers versus sub-heptamers, based on the particle heights, one would surmise that both forms exhibit the propensity to coalesce into trifoliates upon sample-drying. This is evidenced by the recovery of trifoliate-shaped particles from both ~ 2–6 nm height and ~ 10–12 nm height particles (Figure 2 *b* and *c*). It is of interest to note that in the course of this work, a report appeared on dry AFM imaging of helicase DnaG and

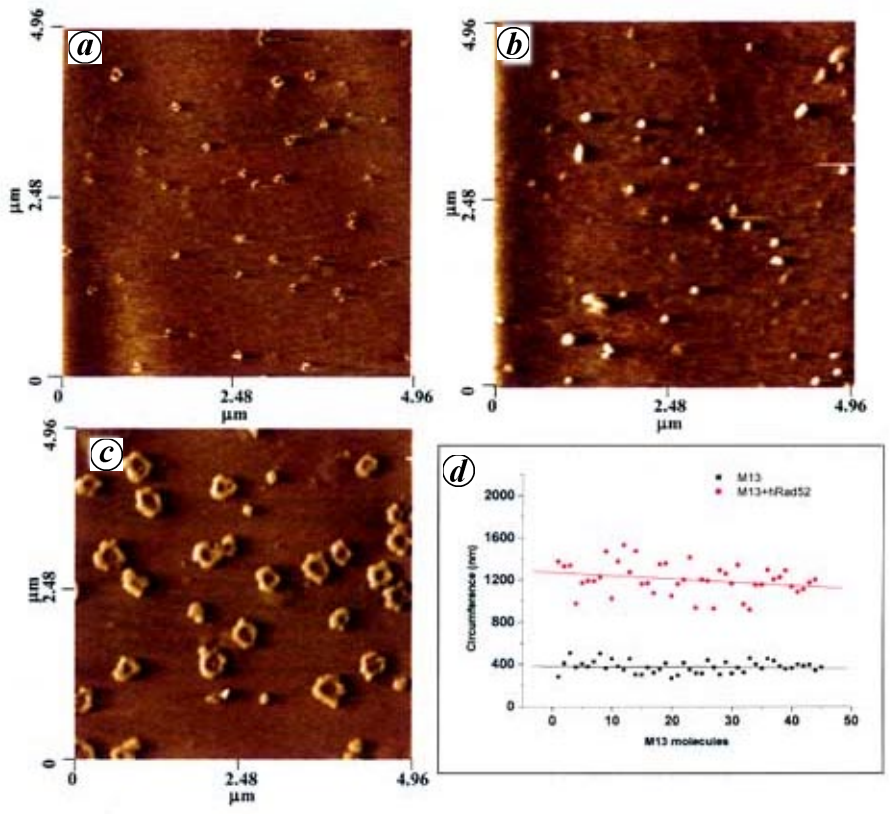

Figure 4. Binding of circular M13-ssDNA molecule in the presence of HsRad52. ***a***, Representative 2D image (5 × 5 µm) of naked circular M13 ssDNA sample. ***b***, A representative 2D image (5 × 5 µm) of naked circular M13 ssDNA following glutaraldehyde fixation. ***c***, Atomic force microscopy imaging of HsRad52 in the presence of circular M13-ssDNA performed under dry conditions. A representative 2D image (5 × 5 µm) of the circular M13 DNA in the presence of HsRad52 after incubation with glutaraldehyde is shown. ***d***, About 45 individual circular molecules in image scans (***a*** and ***c***) were chosen (arbitrarily numbered as 1 to 45) for contour length measurements (see Methods for details), which were expressed as circumferences (in nm) versus the arbitrary number of the molecule analysed. Therefore, each datapoint in the graph represents analyses of separate molecules. Mean contour length is represented by the average line passing through the datapoints of naked (closed squares) (from image ***a***) and HsRad52-coated (closed circles) (from image ***c***) circular M13 molecules.

DnaB molecules, which also indicates the formation of threefold symmetric rings[40]. Importantly, analyses of protein bound to ssDNA fragments reveal particles that are not higher than ~ 5–6 nm and may even encompass smaller ones (Figure 3 *c*–*e*). Only high-resolution AFM imaging can resolve the nature of these particles vis-à-vis that of heptameric and sub-heptameric forms. Notwithstanding this uncertainty, our analyses reveal that HsRad52 protein binding to ssDNA is associated with marked changes in DNA contours, such that the ssDNA backbone gets greatly unfolded (Figure 3 *b* and 4 *c*). We hypothesize that protein binding leads to large-scale disruption of secondary/tertiary structures in ssDNA, thereby rendering the strand sequence highly amenable for pairing by another DNA molecule.

1. Gorbunova, V. and Seluanov, A., Making ends meet in old age: DSB repair and aging. *Mech. Ageing Dev.*, 2005, **126**, 621–628.
2. Friedberg, E. C. and Meira, L. B, Database of mouse strains carrying targeted mutations in genes affecting biological responses to DNA damage. *DNA Repair* (*Amst.*), 2003, **2**, 501–530.
3. Abner, C. W. and McKinnon, P. J., The DNA double-strand break response in the nervous system. *DNA Repair*, 2004, **3**, 1141–1147.
4. West, S. C., Molecular views of recombination proteins and their control. *Nature Rev. Mol. Cell. Biol.*, 2003, **4**, 435–445.
5. Game, J. C. and Mortimer, R. K., A genetic study of X-ray sensitive mutants in yeast. *Mutat. Res.*, 1974, **24**, 281–292.
6. Carney, J. P. *et al.*, The hMre11/hRad50 protein complex and Nijmegen breakage syndrome: linkage of double-strand break repair to the cellular DNA damage response. *Cell*, 1998, **93**, 477–486.
7. Bezzubova, O. Y., Schmidt, H., Ostermann, K., Heyer, W. D. and Buerstedde, J. M., Identification of a chicken RAD52 homologue suggests conservation of the RAD52 recombination pathway throughout the evolution of higher eukaryotes. *Nucleic Acids Res.*, 1993, **21**, 5945–5949.
8. Shinohara, A., Shinohara, M., Ohta, T., Matsuda, S. and Ogawa, T., Rad52 forms ring structures and co-operates with RPA in single-strand DNA annealing. *Genes Cells*, 1998, **3**, 145–156.
9. Singleton, M. R., Wentzell, L. M., Liu, Y., West, S. C. and Wigley, D. B., Structure of the single-strand annealing domain of human

RAD52 protein. *Proc. Natl. Acad. Sci. USA*, 2002, **99**, 13492–13497.
10. Navadgi, V. M., Dutta, A. and Rao, B. J., Human Rad52 facilitates a three-stranded pairing that follows no strand exchange: a novel pairing function of the protein. *Biochemistry*, 2003, **42**, 15237–15251.
11. Bi, B., Rybalchenko, N., Golub, E. I. and Radding, C. M., Human and yeast Rad52 proteins promote DNA strand exchange. *Proc. Natl. Acad. Sci. USA*, 2004, **26**, 9568–9572.
12. Sung, P., Function of yeast Rad52 protein as a mediator between RPA and Rad51 recombinase. *J. Biol. Chem.*, 1997, **272**, 28194–28197.
13. Sugiyama, T. and Kowalczykowski, S. C., Rad52 protein associates with RPA–ssDNA to accelerate Rad51 mediated displacement of RPA and presynaptic complex formation. *J. Biol. Chem.*, 2002, **277**, 31663–31672.
14. Park, M. S., Ludwig, D. L., Stigger, E. and Lee, S. H., Physical interaction between human RAD52 and RPA is required for homologous recombination in mammalian cells. *J. Biol. Chem.*, 1996, **271**, 18996–19000.
15. Mcllwraith, M. J., Van Dyck, E., Mason, J. Y., Stasiak, A. Z., Stasiak, A. and West, S. C., Reconstitution of the strand invasion step of DSB repair using human Rad51, Rad52 and RPA proteins. *J. Mol. Biol.*, 2000, **304**, 151–164.
16. Jackson, D., Dhar, K., Wahl, J. K., Wold, M. S. and Borgstahl, G. E., Analysis of the human replication protein A: Rad52 complex: evidence for crosstalk between RPA32, RPA70, Rad52 and DNA. *J. Mol. Biol.*, 2002, **321**, 133–148.
17. Lloyd, J. A., Forget, A. L. and Knight, K. L., Correlation of biochemical properties with the oligomeric state of human rad52 protein. *J. Biol. Chem.*, 2002, **277**, 46172–46178.
18. Kagawa, W., Kurumizaka, H., Ikawa, S., Yokoyama, S. and Shibata, T. J., Homologous pairing promoted by the human Rad52 protein. *J. Biol. Chem.*, 2001, **276**, 35201–35208.
19. Ranatunga, W., Jackson, D., Lloyd, J. A., Forget, A. L., Knight, K. L. and Borgstahl, G. E., Human Rad52 exhibits two modes of self-association. *J. Biol. Chem.*, 2001, **276**, 15876–15880.
20. Stasiak, A. Z. *et al.*, The human Rad52 protein exists as a heptameric ring. *Curr. Biol.*, 2000, **10**, 337–340.
21. van Dyck, E., Hajibagheri, N. M. A., Stasiak, A. and West, S. C., Visualization of human Rad52 protein and its complexes with hRad51 and DNA. *J. Mol. Biol.*, 1998, **284**, 1027–1038.
22. Kagawa, W., Kurumizaka, H., Ishitani, R., Fukai, S., Nureki, O., Shibata, T. and Yokoyama, S., Crystal structure of the homologous-pairing domain from the human Rad52 recombinase in the undecameric form. *Mol. Cell*, 2002, **10**, 359–371.
23. Pelling, A. E., Sehati, S., Gralla, E. B., Valentine, J. S. and Gimzewsk, J. K., Local nanomechanical motion of the cell wall of *Saccharomyces cerevisiae*. *Science*, 2004, **305**, 1147–1150.
24. Lysetska, M., Knoll, A., Boehringer, D., Hey, T., Krauss, G. and Krausch, G., UV light-damaged DNA and its interaction with human replication protein A: an atomic force microscopy study. *Nucleic Acids Res.*, 2002, **30**, 2686–2691.
25. Umemura, K., Okada, T. and Kuroda, R., Cooperativity and intermediate structures of single-stranded DNA binding-assisted RecA–single-stranded DNA complex formation studied by atomic force microscopy. *Scanning*, 2005, **27**, 35–43.
26. van Noort, J., van der Heijden, T., de Jager, M., Wyman, C., Kanaar, R. and Dekker, C., The coiled-coil of the human Rad50 DNA repair protein contains specific segments of increased flexibility. *Proc. Natl. Acad. Sci. USA*, 2003, **100**, 7581–7586.
27. Chang, Y. C., Lo, Y. H., Lee, M. H., Leng, C. H., Hu, S. M., Chang, C. S. and Wang, T. F., Molecular visualization of the yeast Dmc1 protein ring and Dmc1–ssDNA nucleoprotein complex. *Biochemistry*, 2005, **44**, 6052–6058.
28. Tessmer, I., Moore, T., Lloyd, R. G., Wilson, A., Erie, D. A., Allen, S. and Tendler, S. J., AFM studies on the role of the protein RdgC in bacterial DNA recombination. *J. Mol. Biol.*, 2005, **350**, 254–262.
29. Janicijevic, A., Ristic, D. and Wyman, C., The molecular machines of DNA repair: scanning force microscopy analysis of their architecture. *J. Microsc.*, 2003, **212**, 264–272.
30. Wang, H., Bash, R., Yodh, J. G., Hager, G., Lindsay, S. M. and Lohr, D., Using atomic force microscopy to study nucleosome remodelling on individual nucleosomal arrays *in situ*. *Biophys. J.*, 2004, **87**, 1964–1971.
31. Yang, Y., Sass, L. E., Du, C., Hsieh, P. and Erie, D. A., Determination of protein–DNA binding constants and specificities from statistical analyses of single molecules: MutS-DNA interactions. *Nucleic Acids Res.*, 2005, **33**, 4322–4334.
32. Cary, R. B., Peterson, S. R., Wang, J., Bear, D. G., Bradbury, E. M. and Chen, D. J., DNA looping by Ku and the DNA-dependent protein kinase. *Proc. Natl. Acad. Sci. USA*, 1997, **94**, 4267–4272.
33. Gaczynska, M., Osmulski, P. A., Jiang, Y., Lee, J. K., Bermudez, V. and Hurwitz, J., Atomic force microscopic analysis of the binding of the *Schizosaccharomyces pombe* origin recognition complex and the spOrc4 protein with origin DNA. *Proc. Natl. Acad. Sci. USA*, 2004, **101**, 17952–17957.
34. van Noort, S. J., van der Werf, K. O., Eker, A. P., Wyman, C., de Grooth, B. G., van Hulst, N. F. and Greve, J., Direct visualization of dynamic protein–DNA interactions with a dedicated atomic force microscope. *Biophys. J.*, 1998, **74**, 2840–2849.
35. Sattin, B. D. and Goh, M. C., Direct observation of the assembly of RecA/DNA complexes by Atomic Force Microscopy. *Biophys. J.*, 2004, **87**, 3430–3436.
36. Navadgi, V. M., Shukla, A. and Rao, B. J., Effect of DNA sequence and nucleotide cofactors on hRad51 binding to ssDNA: role of hRad52 in recruitment. *Biochem. Biophys. Res. Commun.*, 2005, **334**, 696–701.
37. Navadgi, V. M., Shukla, A., Vempati, R. K. and Rao, B. J., DNA mediated disassembly of hRad51 and hRad52 proteins and recruitment of hRad51 to ssDNA by hRad52. *FEBS J.*, 2005, **273**, 199–207.
38. Parsons, C. A., Baumann, P., van Dyck, E. and West, S. C., Precise binding of single-stranded DNA termini by human RAD52 protein. *EMBO J.*, 2000, **19**, 4175–4181.
39. Van Dyck, E., Stasiak, A. Z., Stasiak, A. and West, S. C., Visualization of recombination intermediates produced by RAD52-mediated single-strand annealing. *EMBO Rep.*, 2001, **2**, 905–909.
40. Thirlway, J. *et al.*, DnaG interacts with a linker region that joins the N- and C-domains of DnaB and induces the formation of 3-fold symmetric rings. *Nucleic Acids Res.*, 2004, **32**, 2977–2986.

ACKNOWLEDGEMENTS. We thank Ashish Shukla and Nabonita Nag for help with the DLS experiments. J.A.D. acknowledges the Homi Bhabha Fellowship Council for award of Homi Bhabha Fellow 2004–06.

Received 4 March 2006; revised accepted 4 September 2006